2nd Science With SALT Workshop, Capetown, S.Africa
*ASP Conference Series, Vol. **VOLUME***, 2003*
ed. D. Buckley

UCRL-PROC-201252

Externally Dispersed Interferometry for Resolution Boosting and Doppler Velocimetry

David J. Erskine

Lawrence Livermore Nat. Lab., 7000 East Ave, Livermore, CA 94550, email: erskine1@llnl.gov

Abstract. Externally dispersed interferometry (EDI) is a rapidly developing technique for wide bandwidth spectroscopy and radial velocimetry. By placing a small angle-independent interferometer near the slit of a spectrograph, periodic fiducials are embedded on the recorded spectrum. The multiplication of the stellar spectrum times the sinusoidal fiducial net creates a moiré pattern, which manifests high detailed spectral information heterodyned down to low spatial frequencies. The latter can more accurately survive the blurring, distortions and CCD Nyquist limitations of the spectrograph. Hence lower resolution spectrographs can be used to perform high resolution spectroscopy and radial velocimetry. A demonstration of $\sim 2\times$ resolution boosting (100,000 from 50,000) on the Lick Obs. echelle spectrograph is shown. Preliminary data indicating $\sim 8\times$ resolution boost (170,000 from 20,000) using multiple delays has been taken on a linear grating spectrograph.

1. Introduction

An externally dispersed interferometer (EDI) is the series combination of an angle-independent Michelson interferometer (Hilliard & Shepherd 1966) with an external grating spectrograph (Fig. 1). The interferometer has a nonzero delay (τ) or optical path length difference, typically 1 to 3 cm, that creates a sinusoidal frequency dependence to its transmission. Inclusion of the interferometer into the light beam, like a filter, embeds (multiplies) a comb of very periodic sinusoidal fiducials on the input stellar spectrum, over the entire spectrograph bandwidth. The EDI therefore has a simultaneous bandwidth advantage over internally dispersed interferometers (Holographic Heterodyning Spectrograph, Spatial Heterodyning Spectrograph) (Douglas 1997; Harlander, Reynolds, & Roesler 1992) which have a limited bandwidth due to a rapid change in fringe periodicity vs wavelength.

Through a heterodyning effect between the fiducials and stellar spectrum, high resolution spectral information forms broad moiré patterns which better survive slit blurring and resist instrumental drifts, allowing use of lower resolution spectrographs. Data reduction arithmetically separates fringing from ordinary spectra components.

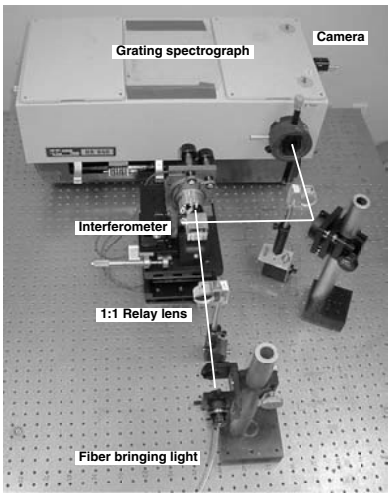

Figure 1. An EDI apparatus using a Jobin-Yvon linear grating spectrograph of ∼20,000 native resolution. The light source (fiber) is imaged to the angle-independent Michelson interferometer mirror plane, where fringes are created. This plane is then imaged to the slit plane of the spectrograph. Due to the nonzero interferometer delay, the fringes have sinusoidal wavelength dependence. This generates a comb of sinusoidal fiducials multiplying the input spectrum, over the entire bandwidth of spectrograph.

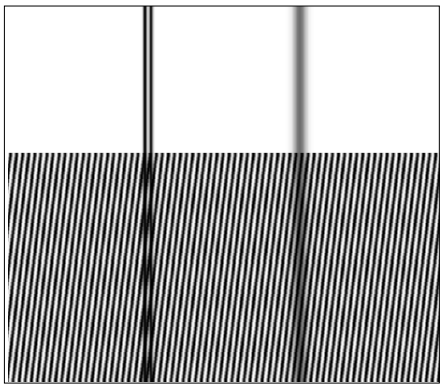

Figure 2. Graphical demonstration of the increased resolving power coming from a heterodyning effect. If viewed from a distance, the doublet of lines on the left in the upper panel appears indistinguishable from the single line on the right. On the bottom panel a sinusoidal pattern is superimposed, representing the interferometer transmission. The presence of the generated moiré pattern immediately distinguishes the doublet. The classic definition of resolving power is ability to distinguish a doublet. Hence the resolution has increased.

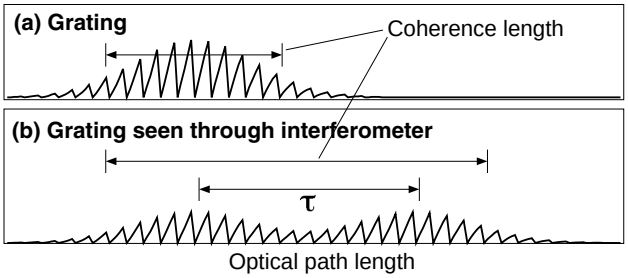

Figure 3. Apparent increase in coherence length of a grating when viewed through an interferometer having delay τ. The spectral resolution is proportional to the grating coherence length. Therefore the resolution of the net device increases.

1.1. Variety of applications

The EDI was originally developed for radial velocimetry (under a Doppler shift the entire moiré pattern shifts in phase). However the EDI's ability to measure precise ($\sim \lambda/20{,}000$) white light fringe shifts between simultaneous multiple spectral sources suggests additional metrology technologies. The EDI has been proposed (Erskine & Edelstein 2003a) to be used with a long baseline interferometer "front end" to measure precision angular differences between simultaneous multiple star targets.

More recently, the EDI's has been applied to high resolution spectroscopy, either as a compact stand-alone instrument, or as performance boosting filter or insert to an existing spectrograph facility. This application is the focus of this article. Essentially, we have "eyeglasses" that can be inserted into the beam path of any spectrograph to boost its spectral resolution by a factor of 2-10$\times$ or more. The EDI can resolve features beyond the Nyquist limit of the CCD, because the moiré patterns encoding the high resolution information are broader than the CCD pixel spacing. Preliminary EDI data indicating an $\sim$8$\times$ resolution boost has been taken recently using multiple interferometer delays observing an iodine spectrum. The EDI also improves spectrograph stability, because the broad moiré patterns are less susceptible to changes in shape of the light beam at the slit, aberrations of spectrograph optics, and mechanical drifts of the CCD.

1.2. Sinusoidal fiducials

In comparison with a dispersed Fabry-Perot interferometer producing narrow impulse spectral fiducial fringes (McMillan et al. 1993), EDI's sinusoidal fiducial fringes transmit greater average flux, provide a heterodyning effect, and allow elegant trigonometric recovery of precise spectral information from as few as three phase-stepped data recordings. The fiducials are easily removed by *summing* the phase stepped exposures, avoiding divide-by-zero issues. The ordinary spectrum is thus recovered along with new information contained in the fringing component. In this sense the EDI's fiducials are "transparent".

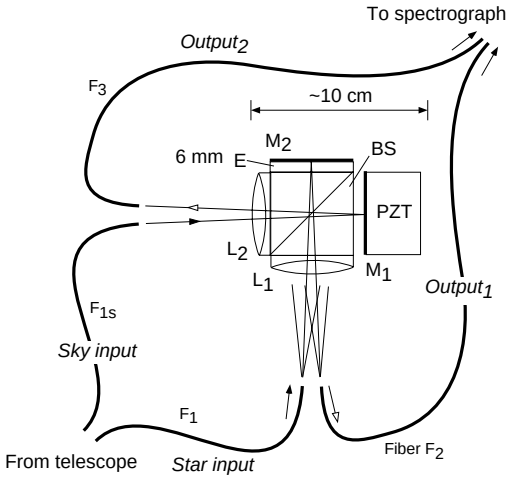

Figure 4. Scheme for a dual input, dual output EDI. Sky fiber F_{1s} produces a fringing signal 180° out of phase with star fiber F_1 and therefore automatically subtracts without using extra CCD pixels. Fibers F_2 and F_3 carrying complementary output signals would go to different positions along spectrograph entrance slit.

1.3. Some Literature

Early EDI radial velocimetry work is described by Erskine & Ge (2000); Erskine (2002); Ge (2003). The first reference demonstrated 1 m/s scale precision in benchtop measurements on laboratory sources. The first EDI stellar radial velocimetry measurements, at the Lick Observatory 1 m in 1999, are described by Ge, Erskine, & Rushford (2002) and have few m/s precision. The EDI has been used to detect the exoplanet around 51 Pegasi at Kitt Peak (Ge et al. 2003).

Two different but related theories for EDI Doppler velocimetry exist, by Ge (2002) and by Erskine (2003). The latter provides a theoretical foundation for the heterodyning effect used in the resolution boosting application, and can be applied to echelle gratings and 1-D imaging spectrographs, as well as linear gratings. That is, the theory handles both uniform and transversely splayed phase along the spectrograph slit.

1.4. Resolution boosting for spectroscopy

Spectral resolution boosting has been demonstrated for echelle and linear grating spectrographs in Erskine & Edelstein (2003b); Erskine et al. (2003). Figure 2 is a graphical demonstration involving a moire effect. An alternative explanation is that the inclusion of the interferometer increases the apparent coherence length of a grating (Figure 3). The spectral resolution ($R \equiv \lambda/\Delta\lambda$) is limited by the latter, which is affected by the slit width and quality of the spectrograph optics. Any object viewed through the interferometer appears twice (with 50% amplitude for each image), but with the second image delayed by τ. The two images of the grating appear as a single grating with a longer coherence length.

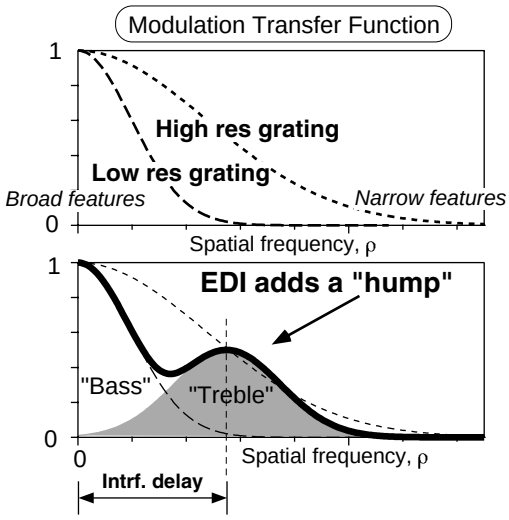

Figure 5. Conventional and EDI instrument transfer functions, i.e. the ability to detect a given spatial frequency (ρ) along the dispersion axis. The interferometer creates a hump in the response.

2. Theory: Conventional spectroscopy

The conventional detected spectrum, $B_{ord}(\nu)$, is the convolution of the input spectrum, $S_0(\nu)$, and the spectrograph line spread function $LSF(\nu)$,

$$B_{ord}(\nu) = S_0(\nu) \otimes LSF(\nu) \tag{1}$$

where frequency is $\nu = 1/\lambda$ in units of cm^{-1}. The full width at half max (FWHM) of $LSF(\nu)$ is $\Delta\nu$ and is related to resolution by $R = \nu/\Delta\nu$. The convolution of Eq. 1 is conveniently expressed in Fourier-space,

$$b_{ord}(\rho) = s_0(\rho)\ lsf(\rho)\ , \tag{2}$$

where lower case symbols are the transformed versions, and ρ is the spatial frequency along the dispersion axis in cycles per cm^{-1}. The $lsf(\rho)$ is thus the transfer function of the impulse response $LSF(\nu)$.

3. Theory: EDI spectroscopy

Figure 4 (section 5.1) shows a scheme for directing both interferometer outputs to spectrograph slit. Then it is appropriate to use the normalized interferometer transmission $T'(\nu)$, which is a sinusoidal spectral comb

$$T'(\nu) = 1 + \gamma \cos(2\pi\tau\nu + \phi)\ , \tag{3}$$

where γ is the interferometer visibility, assumed unity for now, and τ is the nominal interferometer delay in units of cm. Three or four spectra B_ϕ are recorded at phase values ϕ differing by 120° or 90°, respectively, and designated

B_0, B_{90}, etc., so that the phases are distributed evenly around the circle. The ϕ is created by changes in τ, $\phi = 2\pi\Delta\tau$.

The passage of light through the interferometer multiplies the spectral comb $T'(\nu)$ with the input spectrum *prior* to any blurring action from the external grating spectrograph. Hence the EDI detected signal is

$$B_\phi(\nu) = [S_0(\nu)\ T'(\nu)] \otimes LSF(\nu)\ . \tag{4}$$

Equation 4 is re-expressed as a sum of the ordinary spectrum plus two complex counter-rotating fringing terms

$$\begin{aligned} B_\phi(\nu) \quad &= \quad B_{ord}(\nu) + \tfrac{1}{2}[S_0(\nu)e^{i\phi}e^{i2\pi\tau\nu} + \\ &\qquad S_0(\nu)e^{-i\phi}e^{-i2\pi\tau\nu}] \otimes LSF(\nu). \end{aligned} \tag{5}$$

One needs to isolate a single fringing component. To do this, we form a linear combination of data which have been numerically rotated in synchrony with each exposure's phase. This creates a complex (or *vector*) spectrum called a "whirl", $\mathbf{W}(\nu)$. For N-recordings (ϕ evenly spaced)

$$\mathbf{W}(\nu) = \frac{1}{N}\sum B_\phi\ e^{i\phi} \tag{6}$$

and specifically for four exposures every 90°

$$\mathbf{W}(\nu) = \tfrac{1}{4}[(B_0 - B_{180}) + i(B_{90} - B_{270})]\ . \tag{7}$$

Applying Eq. 10 or 7 to Eq. 5 we get

$$\mathbf{W}(\nu) = \tfrac{1}{2}[e^{i2\pi\tau\nu}S_0(\nu)] \otimes LSF(\nu)\ . \tag{8}$$

The Fourier transform of the whirl is

$$\mathbf{w}(\rho) = \tfrac{1}{2}\gamma\ s_0(\rho + \tau)\ lsf(\rho) \tag{9}$$

where we include the interferometer visibility (γ) previously taken as unity.

This important equation describes the EDI formation of moiré fringes, a heterodyning effect expressed in the $s_0(\rho + \tau)$ argument. Fine spectral details having high ρ are heterodyned (shifted by τ) to measurable low ρ prior to any blurring by the spectrograph's line spread function.

Obtaining the ordinary spectrum The ordinary spectrum is obtained from fringing spectra by summing several phase stepped exposures so that the fringing terms cancel,

$$B_{ord}(\nu) = \frac{1}{N}\sum B_\phi \tag{10}$$

or specifically for four recordings

$$B_{ord}(\nu) = \tfrac{1}{4}(B_0 + B_{180} + B_{90} + B_{270})\ . \tag{11}$$

Hence both ordinary and fringing spectra are obtained from the same data set.

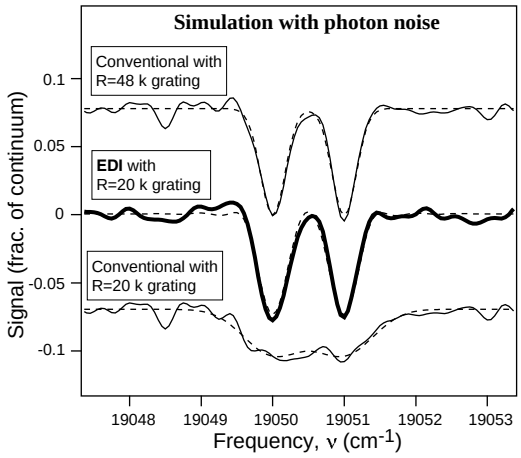

Figure 6. Numerical simulation comparing conventional and EDI techniques in resolving an absorption line doublet under the effect of photon noise. Bold curves include simulated photon noise 1.24% of continuum at pixel size 6 per cm^{-1}.

Heterodyning reversal The heterodyning is reversed by Fourier transforming the data from $\mathbf{W}(\nu)$ to $\mathbf{w}(\rho)$, translating it by τ, and then inverse Fourier transforming it back to ν-space. This procedure is described in more detail in Erskine et al. (2003).

Instrument response Figure 5 shows the transfer function of the conventional and EDI techniques, versus ρ. Higher resolution requires a broader response peak. The EDI response shows a new "treble" peak due to the heterodyning effect, displaced at $\rho = \tau$. By choosing τ to place this peak on the shoulder of the ordinary response ("bass"), the composite EDI response has a high-ρ behavior that approximately matches the conventional technique with a 2.4× higher resolution.

Equalization removes notch The notch in the net EDI response between the bass and treble peaks is removed by changing the weighting of the ρ-components in an equalization step so that the final lineshape is Gaussian. This moderately increases the continuum noise for mid level ρ. Since science features typically reside in the highest ρ of a spectrum, the EDI boost proves useful, as shown in Fig. 6. This numerically simulates the detection of an absorption line doublet by conventional and EDI methods, including equalization, using the same raw CCD "data" containing added random noise simulating photon statistics. The 2.4× boosting effect is confirmed. This also shows that the minor increase in noise for mid-ρ's during equalization does not prevent resolving the doublet, for the 1.24% level of continuum random noise assumed.

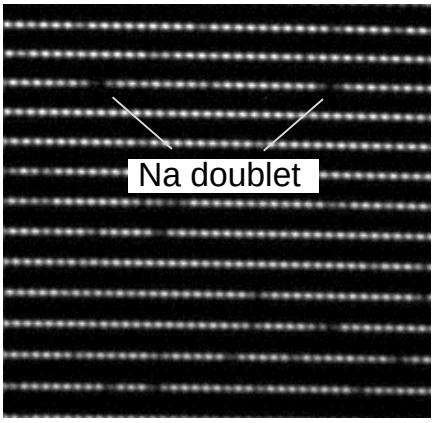

Figure 7. Example EDI echelle CCD data of ϵ-Leo, showing several orders including the sodium doublet. Only a small subset of the full CCD chip is shown. Interferometer creates periodic "bead-like" fiducials.

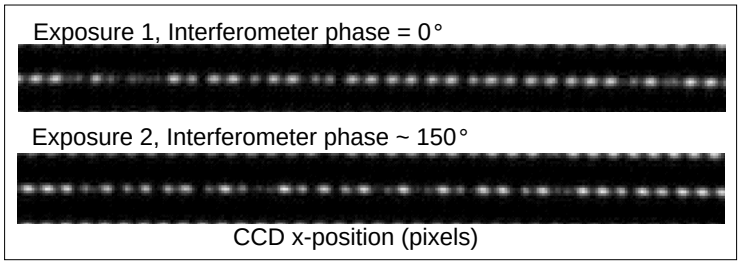

Figure 8. The effect of changing the interferometer phase on a stellar fringing spectrum. Two exposures of the telluric feature near 6868 Å of ϵ-Leo are shown. When the interferometer phase changes 150° between them, the moiré pattern also changes, indicating stellar features similar to the fiducial spacing are present.

4. Example Data

The EDI can be used with ϕ constant or linearly splayed along the slit length. The former allows use with echelle spectrographs and 1-d imaging spectrographs using at least three phase stepped exposures, and the latter allows use with a linear grating obtaining all the needed phase information in a single exposure. Figure 7 shows a section of EDI fringing spectra from the Lick Observatory echelle spectrograph observing ϵ-Leo. The bead-like structure are the sinusoidal fiducials. Figure 8 shows the effect of stepping the interferometer phase observing a single order containing the telluric lines. The change in appearance with phase indicates that the spectrum has structure near the fiducial periodicity, ($\sim$0.9 cm^{-1} for that Figure). Figure 9 demonstrates a $\sim$2$\times$ resolution boosting effect on the echelle (50,000 $\rightarrow$ 100,000) using a 3 cm delay interferometer, comparing conventional and EDI spectra in the telluric region of α-Virgo.

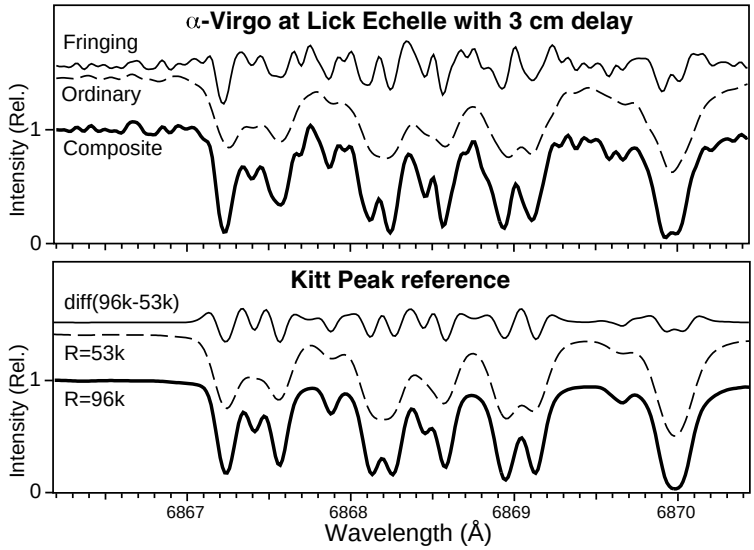

Figure 9. EDI spectral resolution boosting of $\sim 2\times$ is demonstrated for oxygen telluric lines in the Lick echelle spectrum of α–Virgo, (native R=50,000). Bottom: Reference solar spectrum blurred to R=53,000 (dashed line), 96,000 (bold line), and their difference (thin line) compare closely to the EDI spectral components and composite.

5. On-going work: Multiple delay EDI

Figure 10 shows the theoretical response of an EDI using M multiple interferometer delays. Data could be taken sequentially, or in parallel at once with a modified interferometer. Each delay produces a heterodyning peak translated to a different ρ-value so that the concatenate response is extended to $(2M + 1)$ higher ρ than the grating used alone. Hence, after equalization to remove the bumps in the response, the effective resolution can be $(2M + 1)$ times the intrinsic grating resolution. The height of the heterodyned response peaks have been reduced by $\sqrt{M}$ from the ideal single delay value (0.5) to reflect the partition of the same number of photons into M times more exposures.

Experimental work is underway to demonstrate $10\times$ resolution boosting using multiple delays on the linear grating EDI pictured in Fig. 1. Preliminary fringing spectra taken October 2003 of the iodine spectrum using a series of delays detects features up to ∼170,000 resolution, $\sim 8\times$ finer than the ∼20,000 intrinsic resolution of the Jobin-Yvon spectrograph.

In the limit where many discrete delay steps become a continuous scan, multiple delay EDI spectroscopy is related to Fourier Transform spectroscopy (FTS), but has $100\times$ better photon signal to noise ratio over the optical bandwidth. This is due to EDI's use of all the spatial frequencies on the CCD rather than just the DC (constant) component.

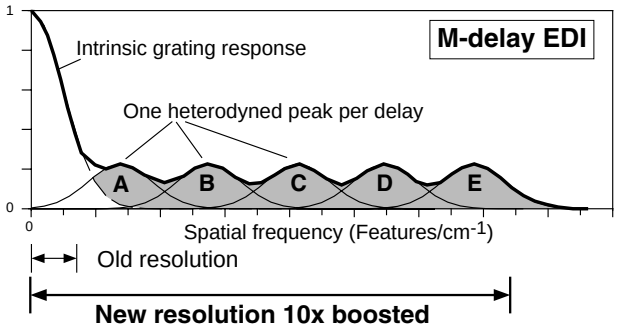

Figure 10. A method of achieving arbitrarily higher spectral resolution is to take a series of exposures at M-different delay values, and concatenate the results.

5.1. Full-pass interferometer designs

To pass all the photons, both complementary interferometer outputs need to be used. Several interferometer designs for providing dual outputs have been identified, some working with open beams and others with fibers. The outputs are directed to slightly different places on the spectrograph slit (otherwise the fringes would cancel). Figure 4 is one example. Schemes for interdigitating the 0° and 180° outputs into the space between echelle orders have been developed. Note, by recording the 0° and 180° data simultaneously, only two separate exposures are needed to provide a full circle of phase steps.

Borrowing an idea from FTS instruments, a complementary output interferometer can also provide complementary inputs, one of which can be assigned to the "sky" so that its fringing output optically subtracts from the primary input. This is a means of automatically subtracting a sky background. (The ordinary spectrum does not have this feature, so this advantage is particularly strong for a multiple-delay EDI where the majority of the signal is fringing. Edelstein (2003) has pointed out that this capability can be used to measure differential velocity fields or differential lineshapes in extended objects.

Acknowledgments. My collaborators Jerry Edelstein, Barry Welsh and Michael Feuerstein of the Space Sciences Lab., Univ. of California, Berkeley assisted in taking the Lick echelle data. Thanks to the Lick Observatory and staff for their facility. Reference iodine spectra were provided by Kitt Peak/NOAO. Work was supported by CalSpace/Lockheed, NASA grants NAG5-9091 and NAG5-3051. This work was performed under the auspices of the U.S. Department of Energy by the University of California, Lawrence Livermore National Laboratory under contract No. W-7405-Eng-48.

References

Douglas, N. 1997, PASP, 109, 151

Edelstein, J. 2003, personal communication

Erskine, D. J. 2002, Combined Dispersive/Interference Spectroscopy for Producing a Vector Spectrum, US Patent Number 6,351,307, issued 26 February 2002

Erskine, D. J. 2003, PASP, 115, 255

Erskine, D. J., & Edelstein, J. 2003a, in SPIE Conf. Proc., 4852, Spectral astrometry mission for planets detection, ed. Michael Shao, 695

Erskine, D. J., & Edelstein, J. 2003b, in SPIE Conf. Proc., 4854, Future EUV/UV and Visible Space Astrophysics Missions and Instrumentation, ed. J. C. Blades, O. H. Siegmund, 158

Erskine, D. J., Edelstein, J., Feuerstein, W. M. & Welsh, B. 2003, ApJ, 592, L103–L106

Erskine, D. J., & Ge, J. 2000, in ASP Conf. 195, Imaging the Universe in Three Dimensions: Astrophysics with Advanced Multi-Wavelength Imaging Devices, ed. W. van Breugel & J. Bland-Hawthorn, 501

Ge, J. 2002, ApJ, 571, L165

Ge, J. 2003, ApJ, 593, L147

Ge, J., Erskine, D. J., & Rushford, M. 2002, PASP, 114, 1016

Ge, J., van Eyken, J., DeWitt, C., & Shaklan, S. 2003, NOAO-NSO Newsletter, March, 73, 31

Harlander, J., Reynolds, R., & Roesler, F. 1992, ApJ, 396, 730

Hilliard, J., & Shepherd, G. 1966, J. Opt. Soc. Am., 56, 362

McMillan, R. S., Moore, T. L., Perry, M. L., & Smith, P. H. 1993, ApJ, 403, 801